Supplementary Materials

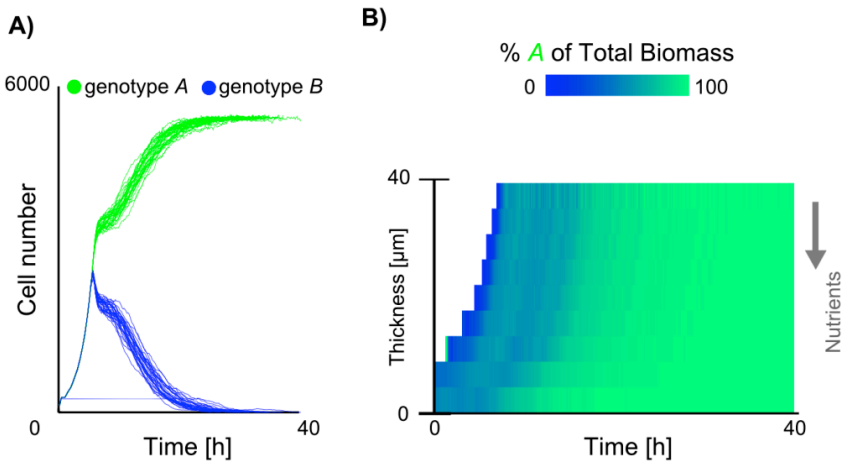

Figure S1: Competition in a model of a nutrient saturated biofilm with saturating nutrients diffusing into the colony from above. A) Cell number over time; initiated with equal cell numbers; genotype *A* outcompetes *B* over time. B) The heat map shows the biomass distribution of the two genotypes averaged over the width of a single simulated biofilm community. Cells grow protected from sloughing in a 40µm thick layer beyond which cells are lost from the biofilm, nutrient concentration N = 4.

Figure S2 and S3: Cell cluster volume expansion can offset the cost of adhesiveness

Our results predict that adhesion is a strategy whose success depends on the localisation of the nutrient source; on the other hand, cell cluster volume expansion is generally beneficial whenever cells live in a structured, nutrient limited environment in which such volume expansion can lead to preferential access to nutrients. Extracellular polymers can either confer adhesiveness to secreting cells (Ma et al. 2006; Vlamakis et al. 2013; Kierek & Watnick 2003) or, conversely, bind to adhesive cell-surface molecules and thus reduce the adhesiveness of secreting cells (Hay et al. 2009; Orgad et al. 2011). These observations suggest that adhesiveness and cell cluster volume expansion can be separately selected over evolutionary time. Our simulations allow us to disentangle the fitness effects of adhesiveness and cell cluster volume expansion, clarifying the separate evolutionary dynamics of these two phenotypic characteristics.

We first consider competition of an adhesive and volume-expanding EPS producer versus a non-producer. Adhesion and volume expansion were shown to independently confer a competitive advantage when nutrients diffuse into the biofilm from the substratum. As expected, these advantages are preserved when the two traits are combined (Figure S2). When nutrients diffuse from above the biofilm, however, our simulations show that the competitive advantage of volume expansion can, depending on position in parameter space, outweigh the potential costs of adhesiveness and the combined-trait genotype outcompetes a non-producer (Figure S2).

In some cases, EPS secretion may reduce cell adhesiveness: for example, alginate secretion *by Pseudomonas aeruginosa* is thought to cover adhesive polymers on the surface of secreting cells (Orgad et al. 2011). To model this potential effect of EPS secretion, we compete the adhesive and volume-expanding genotype against a new genotype *C* that produces volume-expanding EPS but is not adhesive. These simulations recapitulate our previous findings: when nutrients diffuse from above, genotype *C* outcompetes genotype *A* because it can expand towards the nutrient source more readily. When nutrients diffuse into the biofilm from below, adhesiveness allows strain *A* to gain preferential access to nutrients. These results confirm that the evolution of adhesiveness should be strongly influenced by the environment cells are occupying. Whenever limiting nutrients are acquired from the substratum on which biofilms are growing, we predict that cells should evolve to become more adhesive. However, secretion of volume-expanding EPS can help to maintain adhesiveness when nutrients diffuse from above, where adhesiveness alone would be detrimental.

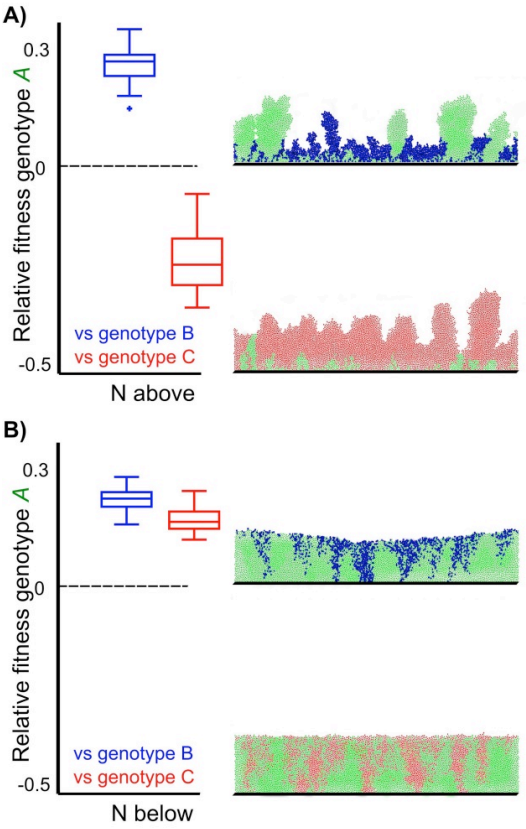

Figure S2: Volume expansion can offset the cost of adhesiveness. Cells of strain *A (*adhesive and volume-expanding due to EPS production) are competed against strain *B* (non-adhesive, non-EPS producing) and species *C* (non-adhesive, but volume expanding due to EPS secretion). A) Nutrients diffuse from above, B) Nutrients diffuse from below. Snapshots of simulations at t = 120h.

Long term evolutionary dynamics of adhesiveness

In the main text, we focus primarily on conditions in which cells grow for a limited period of time defined by a fixed initial supply of nutrients. However, microbes also occupy environments in which nutrients are continuously replenished. Plausible examples include communities on plant roots whose exudates provide nutrition to the resident microbes (Nardi et al. 2000; Narula et al. 2009), riverbeds to which nutrients are constantly supplied from upstream, and the mammalian gut in which large amounts of complex carbohydrates are secreted by the epithelium to feed and potentially select beneficial microbial species (Bevins & Salzman 2011; Hooper et al. 1999). We modified our model to better capture such communities by allowing communities to grow over much longer time scales, and we also implemented a sloughing mechanism whereby cells are lost from the biofilm once they reach a defined height. Our findings are unaffected by these conditions: EPS production is competitively advantageous whenever concentrations of nutrients are low. On the other hand, the fitness effect of adhesiveness still depends on the direction from which nutrients diffuse into the biofilm: highly

adhesive cells outcompete non-adhesive cells when nutrients diffuse from the substratum, but highly adhesive cells are outcompeted when nutrients diffuse from above the biofilm (Figure S3).

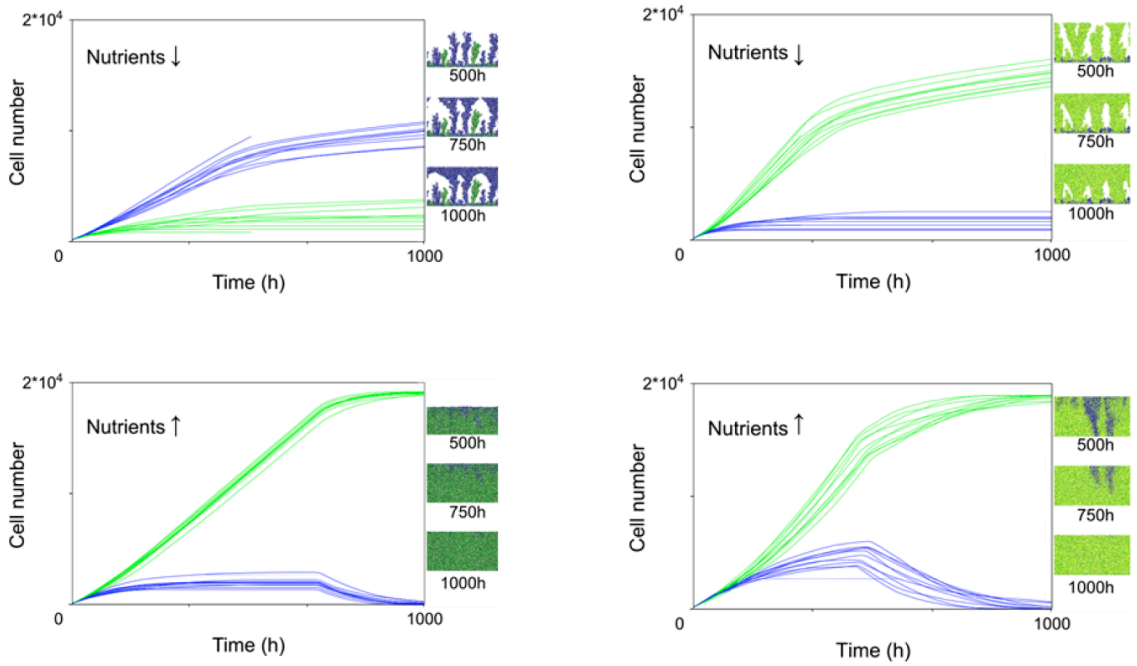

Figure S3: Adhesion and volume expansion in long-term microbial communities. Left: adhesive genotype *A* (green) competes with non-adhesive genotype *B* (blue). Right: EPS producing species *A* competes against non-producing genotype *B.* Plots show cell numbers over time and representative snapshots of three time points. Cells are sloughed from the biofilm surface at a defined height of 150µm.

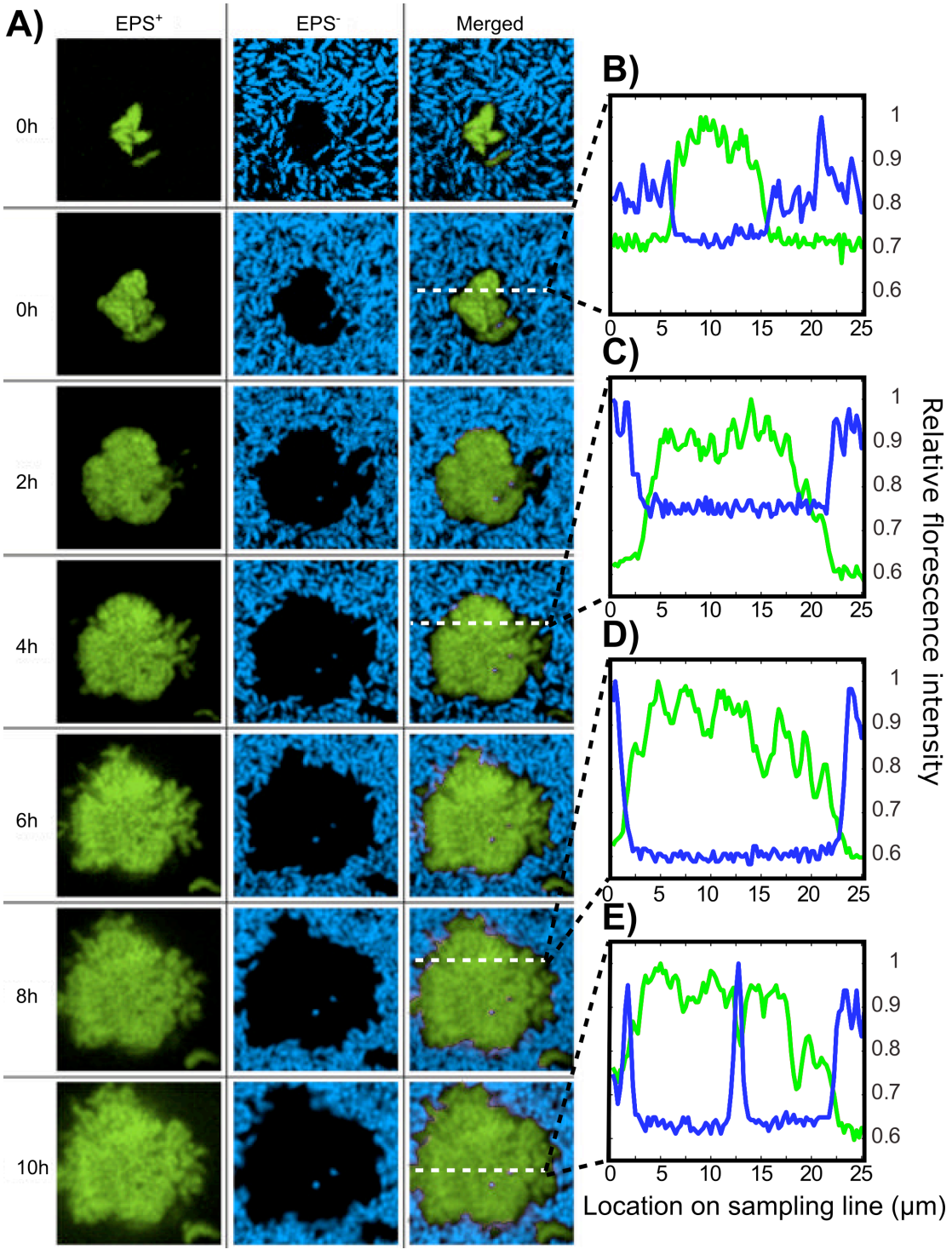

Figure S4: An EPS$^+$ cell cluster displaces EPS$^-$ cells along the glass substratum of a microfluidic device. A) A 24 h time series with images taken at 4h intervals (top to bottom). An EPS$^+$ cluster (green) expands laterally on glass, replacing EPS$^-$ cells (yellow) along its advancing front (each image is 25 x 25 μm). Split channel micrographs are shown for clarity of interpretation (left column: EPS$^+$ cells; middle column: EPS$^-$ cells) in addition to merged images like those shown in Figure 6 of the main text (right column). At t = 4h (B), 12h (C), and 20h (D), fluorescence intensities in both the EPS$^+$

and EPS^- channels are shown along a 1-pixel row 10 μm from the top of the focal imaging area, illustrating the expansion of the focal EPS^+ cluster and corresponding retreat of the EPS^- cell monolayer surrounding it. Fluorescence intensities are normalized to their maximum value in the focal micrograph. Most often, EPS^- cells are cleared from the glass as the EPS^+ cluster expands. E) A fluorescence intensity trace along a new horizontal sampling line illustrates that on occasions when EPS^- are trapped underneath expanding EPS^+ clusters, they are readily detectable (note the spike in EPS^- fluorescence at approximately 13 μm).

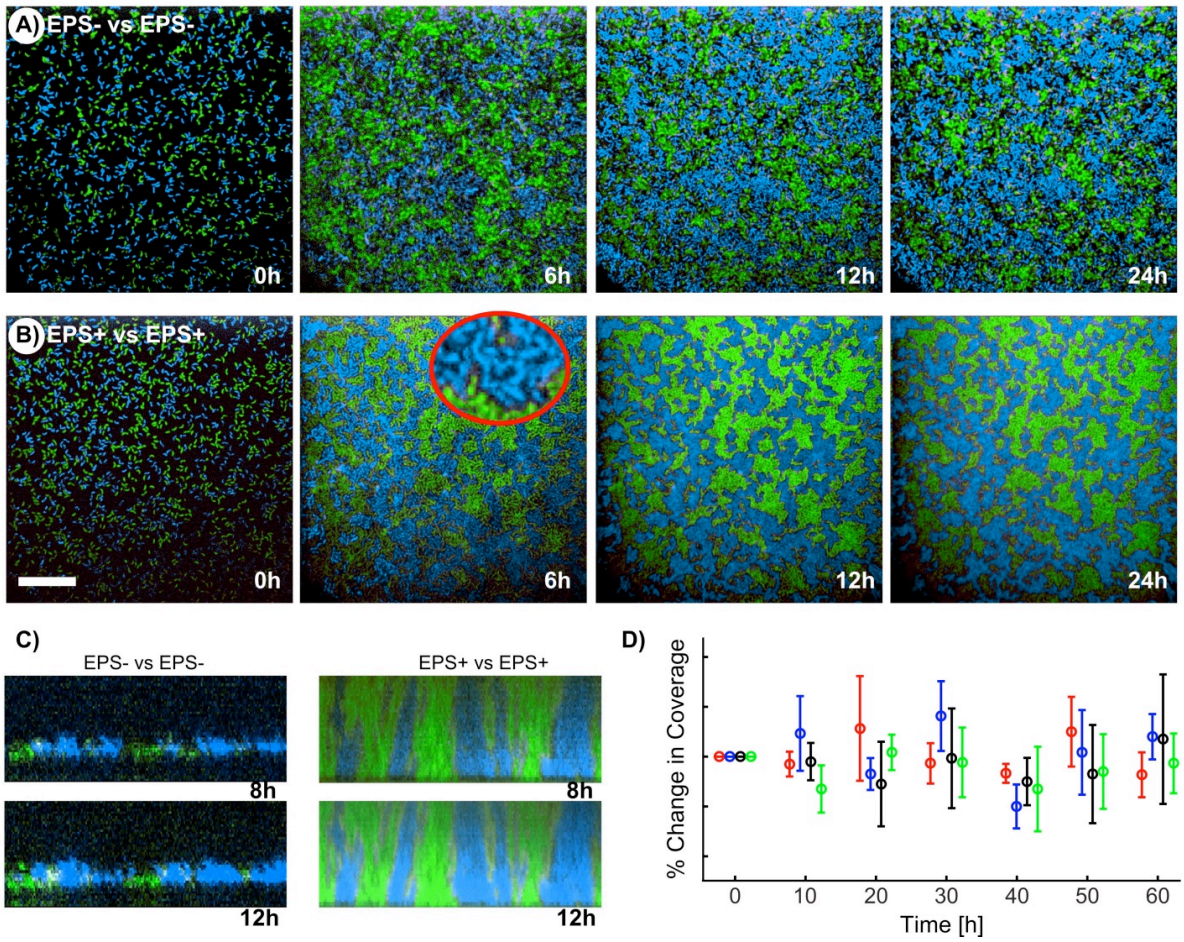

Figure S5: Control experiments. A) A time series for the bottom layer of EPS^- (green) competing against other EPS^- cells (blue). B) A time series for the bottom layer of EPS^+ (green) competing against other EPS^+ cells. Inset at 6h: a digital zoom shows tight packing of cells in EPS^+ colonies. C) Cross-sections of EPS^- (blue) vs. EPS^- (green) and EPS^+ (blue) vs. EPS^+ (green) show no clear displacement. D) Resistance to shear by monocultures of EPS^+ and EPS^- cells. Glass slides were colonized with either strain and exposed to two different flow rates, and surface coverage was measured at 10 min intervals for 1 h. Analysis of surface coverage by EPS^+ (red: 400 µm /sec flow; blue: 20 µm /sec flow) and EPS^- cells (black: 400 µm /sec flow, green: 20 µm/sec flow) indicates that both are capable of forming and maintaining monolayers in the presence of flow.

Table S1) Simulation parameters. Length (L), mass (M), time (T).

Symbol	Description	Dimen-sion	Value	Units	References
Max. colony thickness gut simulations		L	40	µm	(Schluter & Foster 2012)
Max. cell radius before division		L	1	µm	(Mitri et al. 2011)
Width of simulated colony		L	350	µm	
Initial cell number (*A*+*B*), unless stated otherwise			280		
Boundary layer thickness		L	100	µm	
μ	maximum growth rate	T^{-1}	1	h^{-1}	(Mitri et al. 2011; Rang et al. 1999)
K_N	Half saturation constant for growth on nutrient *N* and *L*	ML^{-3}	$3.5*10^{-5}$	gl^{-1}	(Mitri et al. 2011; Nadell et al. 2010)
D	Diffusion coefficient of solutes	L^2T^{-1}	$5.76*10^4$	μm^2h^{-1}	(Nadell et al. 2010)
N	Bulk nutrient concentration	ML^{-3}	$5*10^{-4}$	gl^{-1}	(Nadell et al. 2010)
ρ_X	Density of biomass	ML^{-3}	220	gl^{-1}	(Mitri et al. 2011)
ρ_{EPS}	Density of EPS	ML^{-3}	As a fraction of ρ_X	gl^{-1}	(Mitri et al. 2011)
Y	Yield of biomass per substrate		0.5		(Mitri et al. 2011)
f_{EPS}	Fraction of growth diverted into EPS production		0.25		
σ	Adhesion parameter		2 when adhesive, 1 otherwise	dimen-sionless	
r	Sloughing parameter		0: no sloughing 0.1: weak sloughing 20: strong sloughing		
	Maximum allowed biomass in nutrient limited simulations	M	10^{-8}	g	

Table S2) Stoichiometry of microbial growth and EPS secretion

Reaction	**Solute**	**Biomass**		**Rate Expression**
	N	**Cell biomass (X)**	**EPS**	
growth	-1/Y	$1 - f_{EPS}$	f	μ [N] / ([N] + K_N) X

Text S1

In the following we provide a detailed explanation of the implementation of adhesion in our model concerning the differential rates of displacement. We relate this to conventional viscous draft calculations of spheres in viscous liquids.

In our simulations, cells are moved between each simulation timestep so as to remove any overlap caused by growth and division. Each cell's net movement is the vector sum of displacements induced by overlapping neighbours. For clarity, an overview in pseudocode the shoving algorithm performs the following steps:

Let $\mathbb{L}$ be a list of all cells in random order;
while *total overlap > 0* **do**
  for *focal cell* $C_i \in \mathbb{L}$ **do**
    Let the set of current neighbours of C_i be $\mathbb{J}_i$;
    Reset displacement vector: $(\vec{s}_{C_i}) = \vec{0}$;
    for *neighbour* $j \in \mathbb{J}_i$ **do**
      Calculate displacement vector: $\vec{s}^{\,k}_{i,j} = \underbrace{(R^{\mathrm{O}}_{i,j})_k}_{\text{overlap}} \times \overbrace{(\hat{v}_{j,i})_k}^{\text{vector opposite to overlap between } C_i, j}$;
      Add displacement vector to sum: $(\vec{s}_i)_k \to (\vec{s}_i)_k + \vec{s}^{\,k}_{i,j}$;
    end
    Update position of focal cell C_i: $\vec{x}_i \to \vec{x}_i + (\vec{s}_i)_k$;
    if $(\vec{s}_i)_k \neq \vec{0}$ **then** total overlap $+= 1$;
  end
end

We next introduce a weighting factor $dV_{i,j}$, given by

$$dV_{i,j} = \begin{cases} \frac{2\sigma_j}{\sigma_i+\sigma_j} & \text{if } \sigma_i > \sigma_j, \\ 1 & \text{if } \sigma_i \leq \sigma_j, \end{cases} \tag{1}$$

where σ_i is the dimensionless adhesion parameter for cell i. This weighting factor is applied when calculating the j-th component of a focal cell's displacement vector,

$$\vec{s}^{\,k}_{i,j} = (dV_{j,i})(R^{\mathrm{O}}_{i,j})_k(\hat{v}_{i,j})_k, \tag{2}$$

where $(dV_{i,j})_k$ is a weighting factor, $(R^{\mathrm{O}}_{i,j})_k$ is the overlap between cells i, j, and $(\hat{v}_{j,i})_k$ is a unit vector pointing from cell j to cell i, all defined for the kth shoving step.

The purpose of this weighting factor is to capture the effects of cell adhesion to the biofilm matrix in which all cells are assumed to be embedded and which anchors the biofilm to the surface. For this aspect of our implementation of adhesion, we assume that cell can have different adhesive molecules on their surface that binds them strongly or less strongly to the matrix. Cells that adhere more strongly to the biofilm matrix are expected to move less on average than those that adhere less stongly.

We next demonstrate

- the effects of movement weighting, and show that adhesion parameters σ_i can be used to control the relative movement of cells (§1);
- a physical interpretation of the adhesion parameters, in terms of effective viscosities (§2).

§1 Adhesion parameters σ_i control average cell movement

Using the movement weighting given in Equation (2), the distance s_i moved by an individual cell i in a given timestep can be written as a sum

$$s_i = \left| \underbrace{\sum_{k}^{K} \overbrace{\left(\sum_{j}^{J} (dV_{ij})(\vec{s}_{ij})_k \right)}^{\text{sum over J neighbours}}}_{\text{sum over K shoving steps}} \right|, \tag{3}$$

where $(|\vec{s}_{ij}|)_k$ is the length of the *unweighted* displacement of cell i resulting from contact with neighbour j, during the kth step of the shoving process, and $(dV_{i,j})$ is the weighting factor for an i,j pair. Figure ST1 shows the calculation of $(\vec{s}_{ij})_k$ for a simple arrangement of cells.

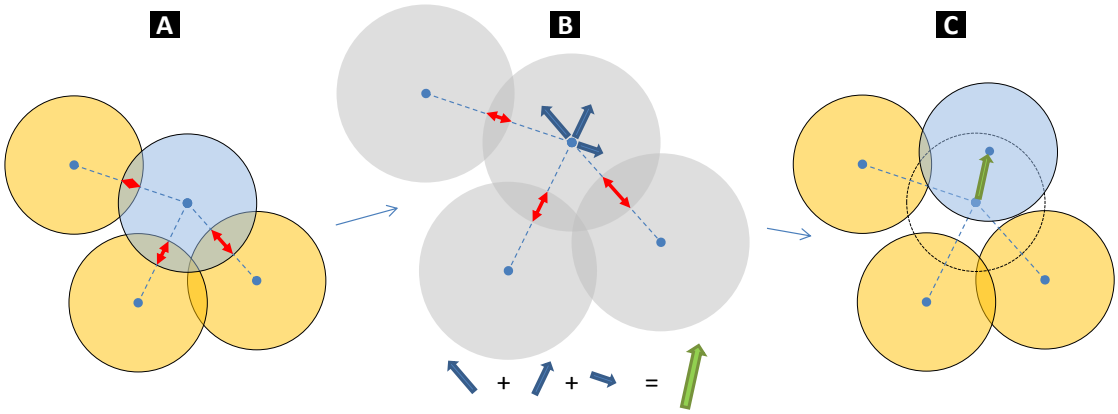

Figure ST1: Cartoon showing the calulation of a displacement vector for a randomly-chosen focal cell (in blue) overlapping with one or more neighbour cells (in yellow).

Using Equation (3), we now show how the weighting factors $dV_{i,j}$ govern average cell movements in a population of cells with different adhesivities. Consider a biofilm consisting of

i. N_A cells with adhesion parameter σ_A;

ii. N_B cells with adhesion parameter σ_B.

If we wish to know how far, on average, cells of type A are moving relative to type B as a function of their adhesion parameter σ_A, we can define a displacement average over each subpopulation

$$\langle s \rangle_X = \frac{1}{N_X} \sum_{n}^{N_X} s_n, \quad X = [A, B], \tag{4}$$

$$= \frac{1}{N_X} \sum_{n}^{N_X} \left| \sum_{k}^{K} \left(\sum_{j}^{J} (dV_{ij})_k (\vec{s}_{ij})_k \right) \right|. \tag{5}$$

Two types of cells are present, so weighting factors $dV_{i,j}$ can take on two values:

i. dV_{XX} for like cell pairs,

ii. dV_{XY} for unlike cell pairs,

so Equation (5) can be rewritten in partitioned form

$$\langle s\rangle_X = dV_{XX}\underbrace{\left(\frac{1}{N_{XX}}\sum_n^{N_{XX}}\left|\sum_k^K\sum_j^J(s_{i,j})_k\right|\right)}_{\text{unweighted av.; like pairs}} + dV_{XY}\underbrace{\left(\frac{1}{N_{XY}}\sum_n^{N_{XY}}\left|\sum_k^K\sum_j^J(s_{i,j})_k\right|\right)}_{\text{unweighted av.; unlike pairs}} \tag{6}$$

$$= dV_{XX}\langle s\rangle_{XX} + dV_{XY}\langle s\rangle_{XY} \tag{7}$$

When cell numbers are equal, the unweighted averages $\langle s\rangle_{XX}$ and $\langle s\rangle_{XY}$ will be the same as without weighting, cells will tend to be shoved by neighbouring cells similarly, regardless of their type. Thus, all changes to absolute movements are solely due to differences in the adhesion parameters and the resulting differential movement weighting.

This means that the ratio of averages is given by

$$\frac{\langle s\rangle_A}{\langle s\rangle_B} = \frac{dV_{AA}\langle s\rangle_{AA} + dV_{AB}\langle s\rangle_{AB}}{dV_{BB}\langle s\rangle_{BB} + dV_{BA}\langle s\rangle_{BA}} \tag{8}$$

$$= \frac{dV_{AA} + dV_{AB}}{dV_{BB} + dV_{BA}} \tag{9}$$

$$= \frac{1 + dV_{AB}}{1 + dV_{BA}} \tag{10}$$

A graph of $\langle s\rangle_A / \langle s\rangle_B$ against the adhesion parameter ratio $\sigma_B/\sigma A$ is shown in Figure ST2.

If $\sigma_A < \sigma_B$, then $dV_{AB} = 1$ and $dV_{BA} = 2\sigma_A/(\sigma A + \sigma B) < 1$, so

$$\frac{\langle s\rangle_A}{\langle s\rangle_B} = \frac{2}{1 + \left(\frac{2\sigma_A}{\sigma_A+\sigma_B}\right)} > 1, \tag{11}$$

i.e. on average, cells of type A will move further than cells of type B each simulation timestep, if their adhesion parameter is set to be lower than that for type B cells.

Conversely, if $\sigma_A > \sigma_B$, then $dV_{BA} = 1$ and $dV_{AB} = 2\sigma_B/(\sigma A + \sigma B) < 1$, giving

$$\frac{\langle s\rangle_A}{\langle s\rangle_B} = \frac{1 + \left(\frac{2\sigma_B}{\sigma_A+\sigma_B}\right)}{2} < 1, \tag{12}$$

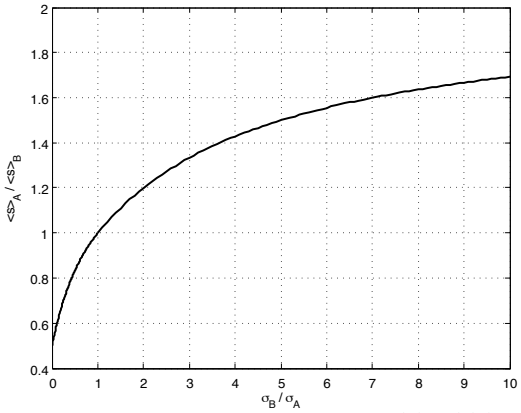

Figure ST2: Graph of ratio of average cell displacements $\langle s\rangle_A / \langle s\rangle_B$ against adhesion parameter ratio $\sigma_B/\sigma A$.

i.e. cells of type A will move less far than cells of type B, if their adhesion parameter is set to be greater.

Finally, if the two cells are equally adhesive such that $\sigma_A = \sigma_B$, all weighting factors $dV_{AA} = dV_{BB} = dV_{AB} = dV_{BA} = 1$, and we obtain

$$\frac{\langle s \rangle_A}{\langle s \rangle_B} = 1. \tag{13}$$

In this way, use of movement weighting factors $dV_{i,j}$ allows the relative mobility of cells to be controlled through the parameters σ_A and σ_B.

§2 Adhesion parameters σ_i are proxies for effective viscosities μ_i

In this section we use physical arguments to demonstrate the mapping between the adhesion parameters σ_i and the viscosity of the biofilm matrix for cells of different adhesiveness. This makes three assumptions about a configuration of cells in a biofilm:

i. Repulsive forces $\vec{F}_{\text{rep}}$ exist between cells in mechanical contact, generated by the deformation of cell walls.

ii. These repulsive forces are always in equilibrium with viscous drag forces $\vec{F}_{\text{drag}}$. These are given by Stokes' law, $\vec{F}_{i,\text{drag}} = -6\pi\mu R_i \vec{v}_i$, where μ is the effective viscosity of the aurrounding matrix experienced by cell i, R_i is its radius, and $\vec{v}_i$ its velocity.

iii. Adhesive interactions between cells and biofilm matrix alter cell motion only by affecting μ.

With these assumptions, we can write the displacement of a cell $\vec{s}_i$ over a time period Δt as the integral of that cell's velocity, $\vec{v}_i = -\vec{F}_{i,\text{drag}}/6\pi\mu_i R_i$,

$$\vec{s}_i = -\frac{1}{6\pi\mu_i}\int_0^{\Delta t} \frac{\vec{F}_{i,\text{drag}}}{R_i} dt = \frac{1}{6\pi\mu_i}\int_0^{\Delta t} \frac{\vec{F}_{i,\text{Tot}}}{R_i} dt, \tag{14}$$

where for the second step we have used our overdamping assumption, $\vec{F}_{i,\text{Tot}} = -\vec{F}_{i,\text{drag}}$.

As in the previous section (Equations (4) and (6)), we consider a population comprised of two types of cells,

i. N_A cells with effective viscosities μ_A;

ii. N_B cells with effective viscosities μ_B.

Each cell type $X = [A, B]$ will have an associated average displacement $\langle s \rangle_X$, and the ratio of these averages will be

$$\frac{\langle s \rangle_A}{\langle s \rangle_B} = \frac{\frac{1}{N_A}\sum_a^{N_A} |\vec{s}_a|}{\frac{1}{N_B}\sum_b^{N_B} |\vec{s}_b|}, \tag{15}$$

$$= \frac{\left(\frac{1}{6\pi\mu_A}\right)\frac{1}{N_A}\sum_a^{N_A}\left(\int_0^{\Delta t}\frac{|\vec{F}_{a,\text{Tot}}|}{R_a}dt\right)}{\left(\frac{1}{6\pi\mu_B}\right)\frac{1}{N_B}\sum_b^{N_B}\left(\int_0^{\Delta t}\frac{|\vec{F}_{b,\text{Tot}}|}{R_b}dt\right)}, \tag{16}$$

$$= \frac{\mu_B \langle W \rangle_A}{\mu_A \langle W \rangle_B}, \tag{17}$$

where for Equation (17) we define

$$\langle W \rangle_X = \frac{1}{N_X}\sum_x^{N_X}\left(\int_0^{\Delta t}\frac{|\vec{F}_{x,\text{Tot}}|}{R_x}dt\right), \quad X = [A, B]. \tag{18}$$

Key to our argument here is that $\langle W \rangle_A \approx \langle W \rangle_B$, because

- although individual cells may differ in radius R, there is no systematic difference in cell sizes between subpopulations A and B;
- although individual cells will be subject to different net forces $|\vec{F}_{\mathrm{Tot}}|$, there is no systematic difference in the magnitudes of forces exerted in the two subpopulations.

Hence, then we are left with

$$\frac{\langle s \rangle_A}{\langle s \rangle_B} \approx \frac{\mu_B}{\mu_A}. \tag{19}$$

If, for our cell populations, we wish to map the adhesion parameters σ_A, σ_B to the physical constants μ_A, μ_B, we can equate Equations (10) and (19) to give

$$\frac{\mu_B}{\mu_A} \approx \frac{1 + dV_{AB}}{1 + dV_{BA}}. \tag{20}$$

Equation (20) can be used to relate ratios of simulation parameters σ_i to the physical parameters μ_j which govern the viscous drag forces on cells.